Int J Adv Manuf Technol (2016) 82:1707–1714
DOI 10.1007/s00170-015-7474-7

ORIGINAL ARTICLE

Machinability investigations on turning of Cr-Ni-based stainless steel cladding formed by laser cladding process

Peirong Zhang[1,2] · **Zhanqiang Liu**[1,2]

Received: 25 March 2015 / Accepted: 22 June 2015 / Published online: 11 July 2015

Abstract Laser cladding process has been developed to be an advanced surface modification technique in re-manufacturing and maintenance fields. Service performance of the component formed by laser cladding largely depends on its subsequent finish cutting processes. Depth of cut in cladding turning process was restricted relatively small due to the thickness limitation of cladding layer, which reflected distinctive and crucial compared with cutting operations of homogeneous materials. The effect of depth of cut on turning performance of Cr-Ni-based stainless steel formed by laser cladding was investigated in this paper to get a novel insight into the machining process of cladding layer. Larger cutting force, worse surface roughness, and strengthened work-hardening with depth of cut increasing were observed similar to a conventional turning process. However, radial force rather than tangential force dominated especially in the given cutting conditions owing to the shallow depth of cut. Both surface roughness parameters Rz and Rt exhibited twice larger when the depth of cut exceeds 0.18 mm. Furthermore, comprehensive machinability of turning process was quantitatively evaluated based on modified digraph and matrix method so as to obtain a superior functional cladding. The results indicated that the machinability of cladding layer became worse with depth of cut increasing initially. The machinability value reached the worst level with depth of cut equaling to 0.24 mm. Thus, an optimized depth of cut was determined as 0.12 mm for turning of laser cladding Cr-Ni-based stainless steel. It should be noted that tool vibration should be eliminated for improved surface roughness as well as work-hardening with the depth of cut increasing, which performed beneficial to the machining of functional component formed by laser cladding.

Keywords Laser cladding · Cr-Ni-based stainless steel · Turning · Machinability · Depth of cut

1 Introduction

As a surface modification technique, laser cladding has been developed to be an important process in re-manufacturing and maintenance fields, e.g., metallurgy, traffic, petrochemistry, and mining industries [1]. Suitable cladding feedstock with superior physical and chemical properties can save consumption of material resources and energy. They can optimize the part's performance and expand its service life [2, 3]. Laser cladding has been developed for many years as a re-manufacturing and sustainable manufacturing technique in industry [4, 5]. However, laser cladding results in irregular surface and poor dimensional tolerance. It is necessary to machine the cladding layer in a finishing operation to achieve the tight geometric, dimensional, and roughness tolerances required.

Recently, advanced surface modification techniques including high velocity oxy-fuel (HVOF) spraying, arc spraying, and plasma spraying have been applied widely in mechanical fields. Machining processes of such spraying coatings have a similar material removal mechanism with that of cladding layers. These machining operations mainly involve the turning [6–8], milling [9, 10], grinding [11–13], and boring [14, 15] processes. Wang et al. [6, 7] experimentally investigated the influence of cutting parameters on cutting

✉ Zhanqiang Liu
melius@sdu.edu.cn

[1] School of Mechanical Engineering, Shandong University, Jinan 250061, People's Republic of China

[2] Key Laboratory of High Efficiency and Clean Mechanical Manufacture (Shandong University), Ministry of Education, Jinan, People's Republic of China

forces, surface roughness, chip morphology, and tool wear in turning of Fe-based overlay deposited by arc spraying. However, the intrinsic mechanism of coating cutting process was not explained. Furthermore, Sun et al. [8] proposed analytical models in rough and finishing turning of the Fe-Al-based overlays for transient cutting force prediction. Zhao et al. [9, 10] analyzed the chip morphology and machining vibration in end milling and side milling of laser cladding layer. In their research, sawtooth chips were generated on account of low thermal conductance. Machining vibration was considered to be the result of uneven distribution of grain size and hardness, which was effectively improved with La_2O_3 addition. Masoumi et al. [11, 12] investigated the effects of grinding parameters on grinding force and properties including porosity content, residual stress, micro-hardness, and adhesion strength of HVOF sprayed coating. A mechanism of material removal presenting both brittle fracture and ductile flow modes was proposed. The porosity content of the coating increased after grinding, whereas micro-hardness and adhesion strength were reinforced, which resulted from the effects of compressive residual stress states. Rausch et al. [13] optimized a five-axis numerical control (NC) grinding process for improving the surface topographies and shape accuracies prior to industrial application. Ding et al. [14, 15] reported the mechanism of tool wear as abrasive effect by hard oxide particles in boring of plasma-sprayed Fe-based alloys coating. The challenges in machining of cladding or spraying materials are due to their abrasive resistance as well as high hardness and limited thickness of the surface layer.

Even though various researches have been carried out aiming at the machining of cladding layer or spraying coatings, the effects of the shallow thickness of surface cladding layer on cutting processes are less reported. As shown in Fig. 1, materials formed by laser cladding process, which are to be removed by turning process, are crucial difference along radial direction with homogeneous materials formed by other forming processes. The depth of cut is restricted relatively small due to the total thickness limitation of cladding layer. The thickness of the cladding layer is in comparable scale to nose radius of the tool insert applied, similar to a hard turning process.

The influences of depth of cut on turning performances of Cr-Ni-based stainless steel cladding including cutting force, surface roughness, and micro-hardness are investigated in this research. Comprehensive machinability of the series turning processes is further evaluated based on a modified digraph and matrix method. Optimized selection of depth of cut will be determined in cladding turning process.

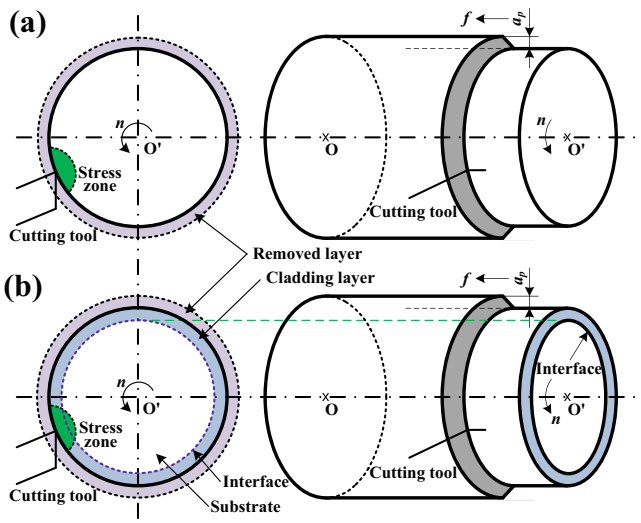

Fig. 1 Comparison between turning processes of **a** homogeneous and **b** laser cladding material

2 Surface preparation and laser cladding process

Figure 2 shows a schematic representation of the laser cladding process. A laser beam is focused and moves on the top surface of substrate for producing a melting pool where a powder flow is injected coaxially. The treated area is heated by absorption of energy delivered by the laser beam. Special powder totally melts and then quickly re-solidifies for creating a track, characterized by high density and metallurgical bonding to the bulk material. Meanwhile, the heated layers consisting of a cladding layer and a heat-affected zone (HAZ) are self-quenched after passing of the laser beam due to diffusion of heat to the cold bulk or air. The high heating and cooling rates result in grain refinement as well as the formation of metastable phases and/or altered microstructures in the surface layer.

The Cr-Ni-based stainless steel cladding was generated on the surface of worn out part, which was fabricated by laser cladding process. Special powder after drying and filter was used as feedstock, while medium carbide steel was used as the bulk material. In this research, a self-designed semiconductor laser cladding equipment was employed for the surface preparation. The substrate material was selected as AISI 1045 steel with a diameter of 40 mm and a length of 90 mm, while the cladding material was Cr-Ni-based stainless steel powder. The compositions of both bulk and cladding material were analyzed by energy disperse spectroscopy (EDS, INCA, Oxford Co.) and is summarized in Table 1. After cladding, the thickness of the cladding layer was approximately 1000–2500 μm, as shown in Fig. 2d. The parameters adopted in laser cladding process are listed in Table 2.

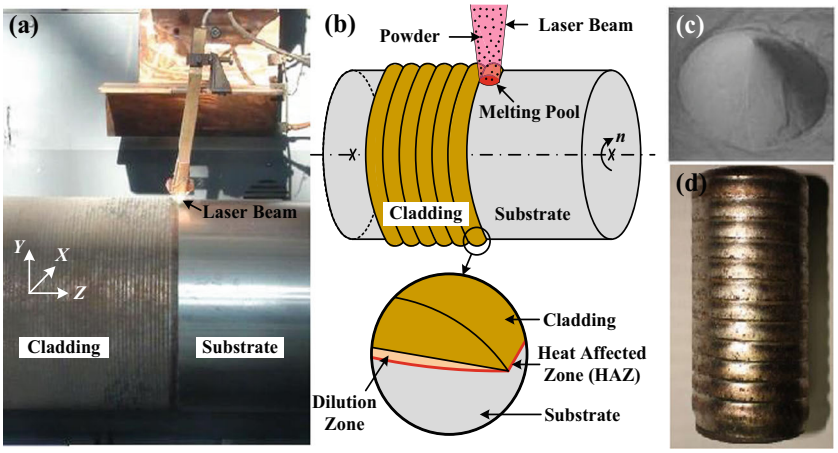

Fig. 2 Schematic representation of the **a** laser cladding equipment, **b** principle of laser cladding process, **c** laser cladding powder, and **d** final shape of the workpiece

3 Experimental details

3.1 Experimental setup and measuring instruments

The effects of depth of cut on cutting force, surface roughness, and micro-hardness were studied through dry turning experiments. All trials were conducted on the DAEWOO PUMA200MA computer numerical control (CNC) turning center, as shown in Fig. 3. The CNC turning center is equipped with a spindle power of 28 kW and a maximum spindle speed of 6000 rpm. Firstly, the original cladding surface was peeled off and the thickness of the removal layer was about 0.3–0.5 mm depending on the cladding quality. Then, the pre-turned surface was grooved with an interval of 10-mm width. The created grooves separated the workpiece into five segments for the subsequent experiments. Each trial was conducted separately between the adjacent grooves. Inserts with wiper-modified geometry were used for improving surface quality of the cladding layer. More detailed characteristic properties of the insert are listed in Table 3.

Cutting force components of radial force (F_x), tangential force (F_y), and axial force (F_z) were measured by Kistler three-component piezoelectric dynamometer during turning process. The values were monitored and recorded through a three-channel charge amplifier with date acquisition system (DynoWare). Surface roughness Ra, Rz, and Rt of machined surface were measured using a TR200-type portable roughmeter. The HVS-1000 digital micro-hardness tester was used to measure the micro-hardness beneath the machined surface to substrate. Measurements of the surface roughness and micro-hardness were tested three times and an average of these values was taken as a response.

Table 1 Chemical compositions of bulk and cladding material

	C	Si	Mn	Fe	Cr	Ni
Bulk (wt%)	0.90	2.77	1.34	94.98	–	–
Cladding (wt%)	1.18	2.65	0.75	83.20	10.10	2.13

3.2 Design of experiments

A single factorial design was adopted in this research so that the independent effect of depth of cut could be investigated explicitly. Five levels of depth of cut were selected covering the spectrum of 0.06–0.3 mm, while cutting speed and feed rate were kept constants as 60 m/min and 0.08 mm/r, respectively.

4 Results and discussion

4.1 Cutting force

Figure 4 shows the relationships between cutting force components and depth of cut. It can be seen that the cutting force components ascend with the increases of depth of cut, which accordingly result in the augmentation of resultant force. Radial force rather than tangential force dominates in experimental conditions because of the shallow depth of cut, which shows a similar trend to the hard turning process as reported in refs. [16, 17]. This phenomenon can be explained by the ploughing effect which prevails under the conditions of comparable depth of cut-to-nose radius. Besides, tangential force nearly catches up with radial force as depth of cut increases. It is preconceived that tangential force will re-dominate when the depth of cut exceeds 0.3 mm.

Table 2 Laser cladding parameters used for surface preparation

Laser power	Scan velocity	Powder feed rate	Carrier gas (N_2) pressure	Footstep
3 kW	5.1 mm/s	450 g/min	0.5 MPa	7 mm

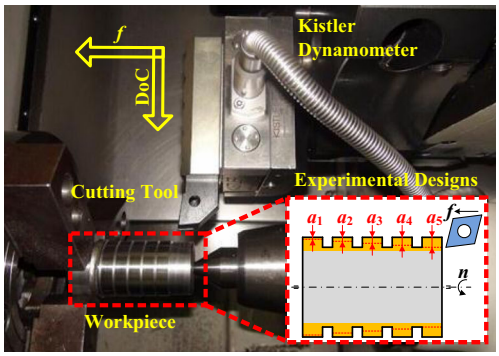

Fig. 3 Experimental setup for cladding turning process

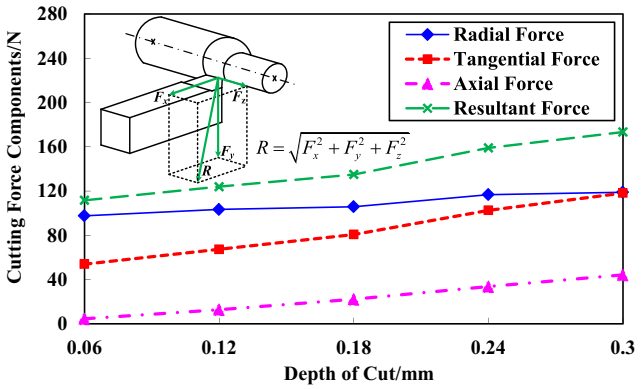

Fig. 4 Relationships between cutting force components and depth of cut

For further comprehension over the variation of cutting force components, the cutting force mechanism in three-dimensional oblique turning process is considered, as shown in Fig. 5. Assuming that the cutting force F_c and the thrust force F_t in orthogonal machining had been derived from shear stress, shear angle, and friction conditions, thus, the tangential, axial, and radial forces can be calculated, respectively, as Eqs. (1)–(3).

$$F_x = \int_{\theta_2}^{\theta_1} (F_t \cos\theta + F_c \sin\lambda_s \sin\theta) R_n d\theta \quad (1)$$

$$F_y = \int_{\theta_2}^{\theta_1} F_c R_n \cos\lambda_s d\theta \quad (2)$$

$$F_z = \int_{\theta_2}^{\theta_1} (F_t \sin\theta - F_c \sin\lambda_s \cos\theta) R_n d\theta \quad (3)$$

where θ represents the position of arbitrary point on cutting edge participated in the turning operation, which will be positive if across the vertical line anticlockwise.

Increasing depth of cut lengthens edge segment participated in the turning procedure, represented by the integral angle θ. The ascending of cutting force can be ascribed to depth of cut increment Δa_p. The thrust force will largely contribute to axial force rather than radial force due to increases of the transient slopes with depth of cut increasing. Thus, the magnitude of axial force increases faster than the radial force as shown in Fig. 4. Besides, longer edge segment participated in the turning procedure enlarges the tangential force according to Eq. (2). In consequence, the tangential force will increase over the radial force overwhelmingly.

Table 3 Detailed properties of turning tooling and coated carbide insert

Tool holder	Coatings	Insert geometrical parameters	
PCLNR2 525M12	Al_2O_3-TiN-TiCN	Side cutting edge angle C_s	−5°
		End cutting edge angle C_e	5°
		Rake angle γ	13°
		Clearance angle α	6°
		Inclination angle λ_s	−7°
		Nose radius R_n	0.8 mm

4.2 Surface roughness

Surface roughness Ra, Rz, and Rt as a function of depth of cut is illustrated in Fig. 6. There is a slight increase in arithmetic mean roughness Ra with depth of cut increasing. This variation could attribute to severe vibration accompanied with screech in the cladding turning processes. Figure 7 shows the optical images of machined surface with typical values of depth of cut. Chatter marks are clearly visible with a high depth of cut, as shown in Fig. 7c, d. The feed marks and vibration deteriorate the surface quality of the machined surface. Besides, surface defects including porosity inherited from laser cladding process and fall-off could also be discovered in the magnification images. Both ductile flow and brittle fracture coexist in the material removal mechanism based on the results of surface observation. Plough effect is another reason for surface deterioration, resulting in severe friction between tool flank face and machined surface. Therefore,

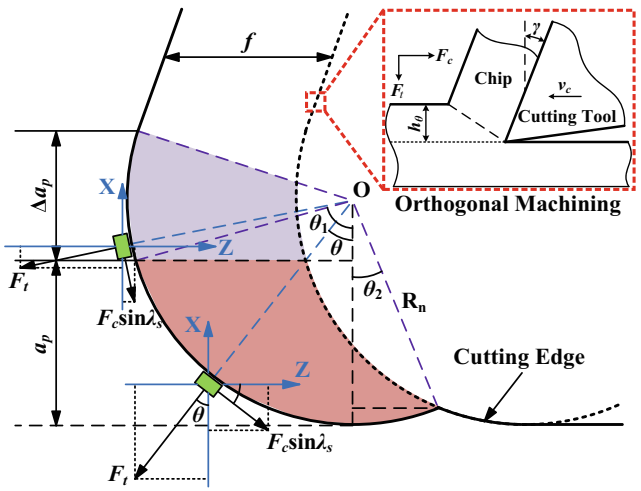

Fig. 5 Cutting force mechanism on the cross section view of undeformed chip

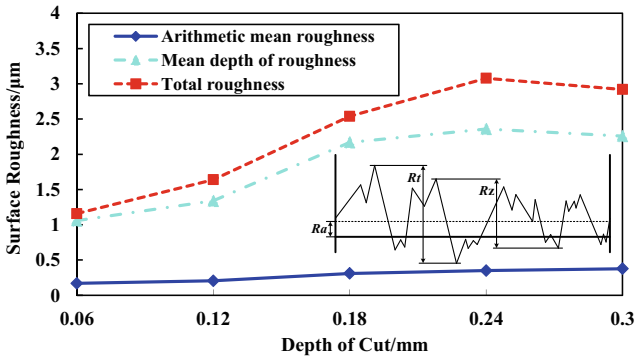

Fig. 6 Effect of depth of cut on surface roughness Ra, Rz and Rt

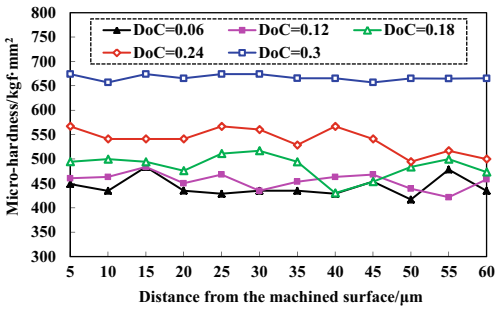

Fig. 8 Micro-hardness of machined subsurfaces with different depths of cut

mean depth of roughness Rz and total roughness Rt exhibit almost twice larger when depth of cut exceeds 0.18 mm under experimental conditions in this research.

A worse surface quality performs detrimentally to usability of the functional cladding layers. Turning inserts with wiper-modified geometry are selected for the purpose of surface improvement. Thereby, it can increase feed rate twice while maintaining the same surface roughness or can reduce surface roughness by half while maintaining the same feed rate when compared to the machined surface by using conventional turning inserts [18–20]. The effect of the interface between cladding layer and substrate should be considered as well. Property differentials between cladding and bulk materials, such as the coefficient of thermal expansion, Young's modulus, and Poisson's ratio, would result in an interfacial residual stress and generating the substrate effect on cladding turning process. Once the depth of plastic deformation reaches the interface or inducing transformation of the interfacial residual stress state, similar to the indention of coatings [21, 22], the substrate effect could not be ignored any longer.

4.3 Micro-hardness

Micro-hardness of the laser cladding samples was measured from top layer of the machined surface till 60 μm beneath the surface. The micro-hardness is recorded with an interval of 5 μm in constant, as shown in Fig. 8. The results indicate a relative stable distribution of micro-hardness in the work-hardening layer. On one hand, the measured micro-hardness of cladding layer is considerably higher than the substrate with an average micro-hardness 250 kgf/mm^2 because of the existence of Cr and Ni elements. On the other hand, increasing depth of cut strengthens the machined surface with an improvement of the micro-hardness. Especially, the micro-hardness increases by 50 % with the maximum depth of cut than that with the minimum depth of cut.

4.4 Machinability evaluation based on digraph and matrix method

Machinability quantifies the machining performance and is defined for a specific application by various indexes, such as cutting force, surface quality, and chip formation. However,

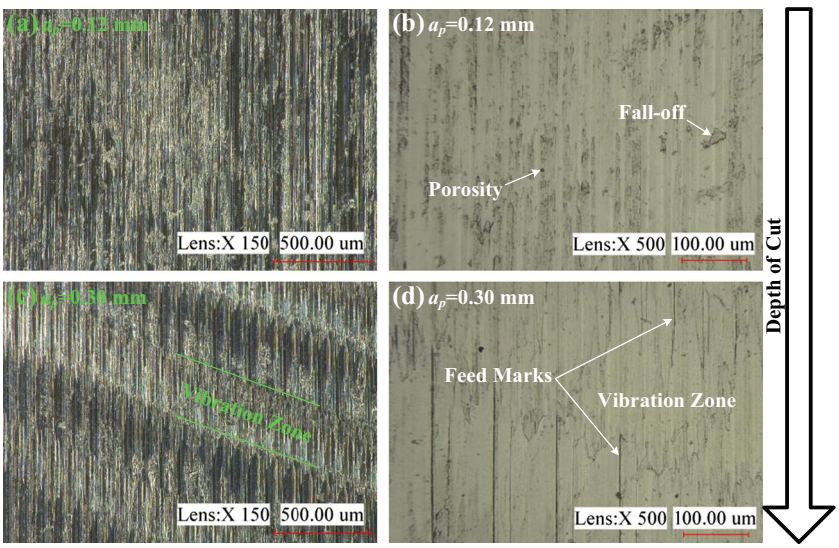

Fig. 7 **a**, **b**, **c**, **d** Optical images of machined surface with a_p= 0.12 mm and a_p=0.30 mm

opposite evaluation values could be obtained with different indexes. Comprehensive machinability considering multiple indexes should be applied for a given machining operation [23, 24]. Digraph and matrix method for machinability evaluation has been developed considering machinability indexes and their relative importance to the operation. This model has been proved useful for modeling and analyzing various kinds of systems and problems in numerous fields of science and technology [25, 26].

4.4.1 Determination of machinability indexes

In this research, resultant force R, mean depth of roughness Rz and micro-hardness Hv are determined as machinability indexes for turning machinability evaluation. Cutting force indirectly reflects the deformation of cladding layer. If the cutting force is large enough, cladding layer could be tore off and inducing catastrophic failure of the functional cladding. Surface quality is the most important factor which affects the performance of functional cladding. The mean depth of roughness could well reflect the topography of the machined surface. With the increment of Rz, more residual spaces storing corrosive medium would be generated which act detrimental to corrosion resistance of the functional cladding. Micro-hardness could induce grain refinement which would be also beneficial to corrosion resistance of the cladding layer.

Firstly, contributes of depth of cut to resultant force, mean depth of roughness, and micro-hardness are determined, respectively, by Eq. (4).

$$\mathrm{Con}\% = \frac{x_{\max} - x_{\min}}{x_{\min}} \times 100\% \tag{4}$$

where $x_{\max}$ and $x_{\min}$ represent the maximum and the minimum value of the machinability indexes, respectively. According to each contribute to the performance of functional cladding shown in Fig. 9, the relative importance of machinability indexes is listed in Table 4.

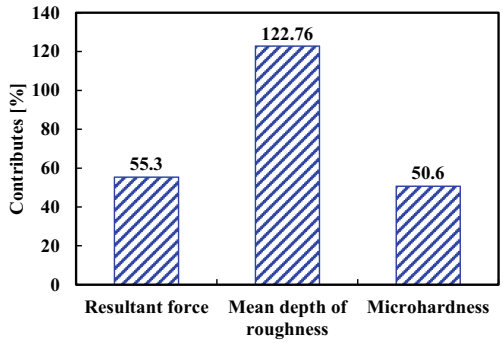

Fig. 9 Contribution values of depth of cut to each machinability index

Table 4 Relative importance of machinability indexes (a_{ij}) for cladding turning processes

Attributes	R	Rz	Hv
R	–	3	5
Rz	7	–	7
Hv	5	3	–

Machinability indexes are dealt with Eqs. (5) and (6). Thus, they are transformed into the closed interval [0, 1], performing the same trend of monotone increment. It is noted that a beneficial index (e.g., micro-hardness) means its higher value is more desirable for the given machining operation, whereas lower value is desirable for a non-beneficial index (e.g., resultant force and mean depth of roughness).

$$\overline{x}_i = \frac{x_i - x_{\min}}{x_{\max} - x_{\min}} \tag{5}$$

$$y_i = \begin{cases} \overline{x}_i \ , & \text{for beneficial index} \\ 1 - \overline{x}_i \ , & \text{for non-beneficial index} \end{cases} \tag{6}$$

where x_i represents the ith value of the machinability indexes. Normalized results of the machinability values are given in Table 5.

4.4.2 Machinability evaluation

Digraph for machinability evaluation of cladding turning processes is developed as shown in Fig. 10. This digraph consists of three nodes 1, 2, and 3 representing resultant force, mean depth of roughness, and micro-hardness, respectively. The relative importance of the above indexes is also illustrated. The comprehensive machinability matrix **A** for this digraph can be written as Eq. (7). This is a 3×3 matrix with diagonal elements y_i and off-diagonal elements a_{ij}. The comprehensive machinability function for the matrix is expressed by Eq. (8).

$$\mathbf{A} = \begin{array}{c} \text{Attributes} \\ R \\ \text{Rz} \\ \text{Hv} \end{array} \begin{array}{c} \begin{array}{ccc} R & \text{Rz} & \text{Hv} \end{array} \\ \begin{bmatrix} y_1 & a_{12} & a_{13} \\ a_{21} & y_2 & a_{23} \\ a_{31} & a_{32} & y_3 \end{bmatrix} \end{array} \tag{7}$$

Table 5 Normalized machinability values (y_i) for cladding turning processes

Depth of cut/mm	R	Rz	Hv
0.06	1	1	0
0.12	0.80	0.78	0.06
0.18	0.64	0.15	0.19
0.24	0.23	0	0.43
0.30	0	0.08	1

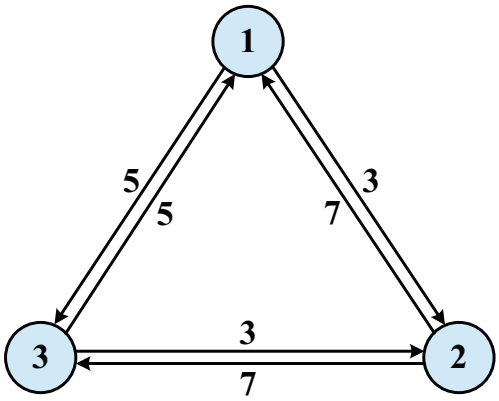

Fig. 10 Digraph for machinability evaluation of cladding turning processes. Machinability indexes: **1** resultant force R, **2** mean depth of roughness Rz, and **3** micro-hardness Hv

$$\text{Machinability}(\mathbf{A}) = \prod_{i=1}^{3} y_i + \sum_{i,j,k} \left(a_{ij}a_{ji}\right)y_k + \sum_{i,j,k} \left(a_{ij}a_{jk}a_{ki} + a_{ik}a_{kj}a_{ji}\right) \quad (8)$$

The comprehensive machinability values for cladding turning processes under different depths of cut are calculated and shown in Fig. 11. Higher machinability value means free machining under corresponding turning parameters. Figure 11 indicates that turning with depth of cut 0.06 mm has the best machinability while that with 0.24 mm is the worst. Machinability value drops down when the depth of cut exceeds 0.18 mm due to worsened surface quality. Thus, vibration should be eliminated for lower surface roughness and stronger work-hardening with the depth of cut increasing, which is beneficial to the machining of functional component formed by laser cladding.

The selection of cutting parameters should consider not only machinability values but also the efficiency of cutting process. Even though the cladding material has the best machinability with the depth of cut 0.06 mm, the efficiency under this condition is the lowest. Therefore, the optimized depth of cut is 0.12 mm with cutting speed 60 m/min as well as feed rate 0.08 mm/r when turning laser cladding material in this study. In this way, the functional cladding component could perform better with a relatively higher efficiency of the cutting process as well.

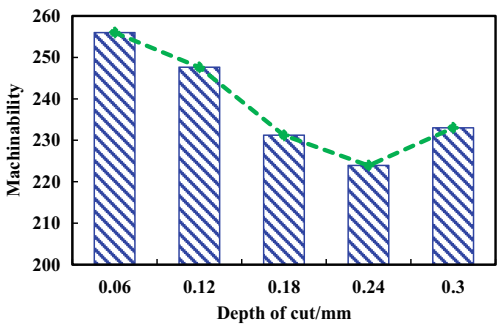

Fig. 11 Comprehensive machinability values for cladding turning processes

5 Conclusions

This research presents the finding of an experimental investigation on the effect of depth of cut on cutting force, surface roughness, and micro-hardness in three-dimensional oblique turning process of Cr-Ni-based stainless steel formed by laser cladding process. The conclusions can be summarized with the cutting conditions in this paper as following:

- Larger cutting force, worse surface roughness, and stronger work-hardening with depth of cut increasing are observed as similar to a conventional turning process. Especially, radial force rather than tangential force dominates in the given conditions owing to shallow depth of cut. In addition, both Rz and Rt exhibit twice larger caused by drastic vibration when depth of cut exceeds 0.18 mm.
- The comprehensive machinability evaluation indicates that machinability becomes worse with depth of cut increasing and reaches the worst when depth of cut is 0.24 mm.
- The optimized depth of cut is 0.12 mm accompanied with the given cutting speed and feed rate for turning of cladding material with better performance and higher efficiency of the cutting process.
- Vibration should be eliminated for improved surface roughness as well as work-hardening with depth of cut increasing, which shows beneficial to the machining of functional component formed by laser cladding process.

A, comprehensive machinability matrix; a_{ij}, relative importance of machinability indexes; a_p, depth of cut (mm); Δa_p, depth of cut increment (mm); C_e, end cutting edge angle (in °); C_s, side cutting edge angle (in °); F_c, cutting force (N); F_t, thrust force (N); F_x, radial force (N); F_y, tangential force (N); F_z, axial force (N); f, feed rate (mm/r); Hv, Vickers micro-hardness (kgf/mm^2); n, rational speed of spindle (r/min); R, resultant force (N); Ra, arithmetic mean roughness (μm); R_n, nose radius (mm); Rt, total roughness (μm); Rz, mean depth of roughness (μm); v_c, cutting speed (m/min); x_i, the ith machinability index; x_{max}, maximum value of machinability indexes; x_{min}, minimum value of machinability indexes; y_i, normalization of the ith machinability index; α, clearance angle (in °); γ, rake angle (in °); λ_s, inclination angle (in °); θ, integral angle (in °).

Acknowledgments The authors would like to acknowledge the financial support from the National Natural Science Foundation of China (Nos. 51425503, 51375272, U1201245) and the Major Science and Technology Program of High-End CNC Machine Tools and Basic Manufacturing Equipment (2014ZX04012014). This work was also supported by grants from Taishan Scholar Foundation.

References

1. Brožek M (2005) Cutting conditions optimization when turning overlays. J Mater Process Technol 168:488–495
2. Tong X, Li FH, Liu M, Dai MJ, Zhou H (2010) Thermal fatigue resistance of non-smooth cast iron treated by laser cladding with different self-fluxing alloys. Opt Laser Technol 42:1154–1161
3. Liu HX, Xu Q, Wang CQ, Zhang XW (2015) Corrosion and wear behavior of Ni60CuMoW coatings fabricated by combination of laser cladding and mechanical vibration processing. J Alloy Compd 621:357–363
4. Liu JC, Li LJ (2004) In-time motion adjustment in laser cladding manufacturing process for improving dimensional accuracy and surface finish of the formed part. Opt Laser Technol 36:477–483
5. Chen CR, Wang Y, Ou HG, He Y, Tang XZ (2014) A review on remanufacture of dies and moulds. J Clean Prod 64:13–23
6. Wang M, Xu BS, Dong SY, Zhang JY, Wei SC (2013) Experimental investigations of cutting parameters influence on cutting forces in turning of Fe-based amorphous overlay for remanufacture. Int J Adv Manuf Technol 65:735–743
7. Wang M, Xu BS, Zhang JY, Dong SY, Wei SC (2013) Experimental observations on surface roughness, chip morphology, and tool wear behavior in machining Fe-based amorphous alloy overlay for remanufacture. Int J Adv Manuf Technol 67:1537–1548
8. Sun YW, Zhang ZJ, Zhang JY, Jin X, Xu BS, Zhao G (2015) Cutting force models for Fe-Al-based coating processed by a compound NC machine tool. Int J Adv Manuf Technol. doi:10.1007/s00170-015-6817-8
9. Zhao YH, Sun J, Li JF (2015) Study on chip morphology and milling characteristics of laser cladding layer. Int J Adv Manuf Technol 77:783–796
10. Zhao YH, Sun J, Li JF (2014) Effect of rare earth oxide on the properties of laser cladding layer and machining vibration suppressing in side milling. Appl Surf Sci 321:387–395
11. Masoumi H, Safavi SM, Salehi M (2014) Grinding force, specific energy and material removal mechanism in grinding of HVOF-sprayed WC-Co-Cr coating. Mater Manuf Process 29:321–330
12. Masoumi H, Safavi SM, Salehi M, Nahvi SM (2014) Effect of grinding on the residual stress and adhesion strength of HVOF thermally sprayed WC–10Co–4Cr coating. Mater Manuf Process 29:1139–1151
13. Rausch S, Biermann D, Kersting P (2014) Five-axis grinding of wear-resistant, thermally sprayed coatings on free-formed surfaces. Prod Eng Res Dev 8:423–429
14. Ding K, Sasahara H, Adachi S, Nishimura K (2010) Investigation on the cutting process of plasma sprayed iron base alloys. Key Eng Mater 447:821–825
15. Ding K, Sasahara H (2012) Study on the machining of iron-based thermal spray coating for sleeveless engine cylinder. Adv Mater Res 472:991–996
16. Tang LH, Gao CX, Huang JL, Lin XJ, Zhang JP (2014) Experimental investigation of the three-component forces in finish dry hard turning of hardened tool steel at different hardness levels. Int J Adv Manuf Technol 70:1721–1729
17. Li Q, Hossan MR (2007) Effect on cutting force in turning hardened tool steels with cubic boron nitride inserts. J Mater Process Technol 191:274–278
18. Guddat J, M'Saoubi R, Alm P, Meyer D (2011) Hard turning of AISI 52100 using PCBN wiper geometry inserts and the resulting surface integrity. Proc Eng 19:118–124
19. Klocke F, Kratz H (2005) Advanced tool edge geometry for high precision hard turning. CIRP Ann Manuf Technol 54:47–50
20. Correia AE, Davim JP (2011) Surface roughness measurement in turning carbon steel AISI 1045 using wiper inserts. Measurement 44:1000–1005
21. Clifford CA, Seah MP (2006) Modelling of nanomechanical nanoindentation measurements using an AFM or nanoindenter for compliant layers on stiffer substrates. Nanotechnology 17:5283–5292
22. Ohmura T, Matsuoka S, Tanaka K, Yoshida T (2001) Nanoindentation load–displacement behavior of pure face centered cubic metal thin films on a hard substrate. Thin Solid Films 385:198–204
23. Olovsjö S, Hammersberg P, Avdovic P, Ståhl JE, Nyborg L (2012) Methodology for evaluating effects of material characteristics on machinability—theory and statistics-based modelling applied on Alloy 718. Int J Adv Manuf Technol 59:55–66
24. Wang XY, Huang CZ, Zou B, Liu HL, Zhu HT, Wang J (2014) A new method to evaluate the machinability of difficult-to-cut materials. Int J Adv Manuf Technol 75:91–96
25. Rao RV, Gandhi OP (2002) Digraph and matrix methods for the machinability evaluation of work materials. Int J Mach Tools Manuf 42:321–330
26. Jangra K, Grover S, Chan FTS, Aggarwal A (2011) Digraph and matrix method to evaluate the machinability of tungsten carbide composite with wire EDM. Int J Adv Manuf Technol 56:959–974